communications earth & environment

Article

A Nature Portfolio journal

https://doi.org/10.1038/s43247-026-03640-7

Rapid and pronounced oceanic deoxygenation fluctuations during the Late Jurassic recorded by thallium isotopes

Check for updates

Elizabeth Atar[1], Andrew C. Aplin[1] ✉, Sean M. Newby[2,3], Seth A. Young[2] & Jeremy D. Owens[2]

The long-term global oxygenation history of ancient oceans provides context for the rapidly decreasing oxygen concentrations in the present-day ocean. Here, we present thallium (Tl) isotope evidence from an epicontinental Laurasian Seaway, deposited during a greenhouse climate between 150 and 149 Ma, that suggests substantial changes in the global burial of manganese (Mn) oxide. This provides evidence for fluctuating global marine (de)oxygenation at a time when there is no evidence for major shifts in the global carbon cycle. Between periods when Tl isotope data suggest similar rates of burial of Mn oxides to the modern, reductions of up to 70% Mn oxide burial are inferred, suggesting major expansions of hypoxic bottom waters. Periods of more extensive global hypoxia are not coincident with regional enrichment of sedimentary organic matter. Fluctuations in deoxygenation occurred on geologically rapid timescales of 10,000 to 100,000 years but are still an order of magnitude lower than those occurring in the modern ocean.

Whilst the present-day ocean is generally well-ventilated, the dissolved oxygen content of the global ocean is decreasing rapidly, by around 2% in the last 50 years[1] and projected to decline by a further 1–7% by 2100[2,3]. Oxygen loss is being driven by (a) the anthropogenic supply of nutrients, resulting in increasing primary productivity and subsequent remineralization and oxygen consumption of biomass; (b) the lower solubility of oxygen in warmer waters and (c) reduced ventilation of the deep ocean as a result of changes in thermohaline circulation patterns[4,5]. This is critical because deoxygenation exerts a profound impact on marine ecosystems, given their sensitivity to even modest changes in oxygen concentrations[6,7] and the subsequent negative feedback of long-term organic carbon burial.

Fluctuations in the oxygenation status of ancient oceans are known and provide important context for studies of the modern ocean. For example, low-oxygen events occurred during a period of abrupt (10^3–10^4 year) warming during the last deglaciation[8], and the Mesozoic sedimentary record documents Oceanic Anoxic Events (OAE) of *ca.* 10^6-year periods of deoxygenation of the global ocean, coinciding with periods of extreme heat and measurable changes in the global carbon cycle[9]. Nevertheless, the response of oceanic oxygen to global warming is poorly constrained and is likely to be complex; for example, a notable reduction in the extent of oxygen-depleted regions of the ocean has been documented in the eastern tropical North Pacific during the warm Middle Miocene and Early Eocene Climatic Optima[10].

These studies imply that past changes in oceanic oxygenation were spatially and temporally heterogeneous, ascribed to variations in nutrient supply, respiration rates and changes in deep ocean ventilation rates[8,10,11]. Regional variations in oxygen concentrations before, during and after Cretaceous OAEs are supported by Earth Systems Models; these suggest that both ocean stagnation and palaeogeography played important roles in spatially variable changes in deep ocean ventilation patterns, with additional variations related to orbital eccentricity cycles[e.g.12–14]. The current response of oceanic oxygenation to warming is thus uncertain, so that assessments of the redox status of ancient oceans during periods of hot climate, both locally and globally, can provide a useful framework for modern deoxygenation studies. Importantly, most of the published work has focused on intervals that have major carbon isotope perturbations which suggest large-scale changes in the carbon cycle, rather than general state changes with small deviations.

[1]Department of Earth Sciences, Durham University, Durham, UK. [2]Department of Earth, Ocean and Atmospheric Science – National High Magnetic Field Laboratory, Florida State University, Tallahassee, FL, USA. [3]Present address: Department of Earth and Planetary Sciences, James Lee Building, The University of Hong Kong, Hong Kong, China. ✉e-mail: a.c.aplin@durham.ac.uk

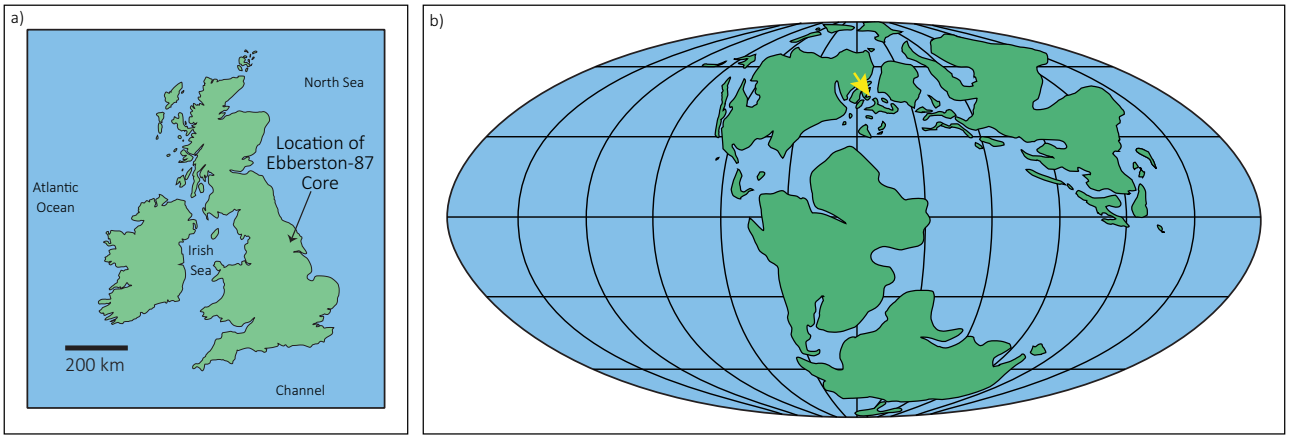

Fig. 1 | Location maps of the study site. a Map of the British Isles showing the location of the Ebberston-87 core in Yorkshire, UK; **b** Global palaeogeographic map of the Late Jurassic, modified after ref. 78. The yellow arrow points to the location of the Ebberston-87 core at the time of deposition.

The local to global redox state of ancient oceans has been commonly inferred from organic-rich shales using both palaeontological and ichnological observations[15,16], and a range of geochemical proxies including trace metal concentrations[17–19], Fe speciation[20,21] and metal isotopes[22–26]. Whilst all shed important light on the related physical, biological, and chemical processes that lead to large-scale organic carbon sequestration in marine sediments, it is the isotopic composition of seawater thallium (ε^{205}Tl) that responds earliest to changes in global marine (de)oxygenation, such as the extent of hypoxia[24,25,27–29].

The isotopic compositions of the known inputs of Tl to the ocean are generally near -2.0 ± 1.0[30] ε-units (or ‰) and are not thought to have varied much through geological time. Temporal variations in seawater ε^{205}Tl therefore reflect changes in oceanic thallium sinks, which are primarily (a) alteration of ocean crust (estimated at 63% removal) with a relatively small isotopic fractionation from seawater ($\Delta^{205}\text{Tl} = -1.2$ ε-units), and (b) sorption by Mn oxides and their preservation in marine sediments (32% removal[24,27,29,30]) with a large isotopic fractionation from seawater ($\Delta^{205}\text{Tl} = \sim+16$ ε-units)[31,32]. Thus, the Mn oxide sink plays a larger role in the temporal variations in ε^{205}Tl, reflecting the extent of Mn oxide preservation. Furthermore, on sub-10^6-year timescales, the rate of alteration of ocean crust can be assumed to be relatively constant as this is likely related to seafloor spreading and should not cause measurable perturbations in ε^{205}Tl; changes in seawater ε^{205}Tl therefore specifically indicate the extent to which Mn oxides are preserved in sediments. More detail on the simple model used to assess controls on ε^{205}Tl in seawater is given in the Methods and in Supplementary Fig. 1.

The seawater residence time of Tl is ~18.5 kyr[30,33], which is long enough for ε^{205}Tl to be homogenous throughout the marine reservoir but short enough to detect rapid changes in (de)oxygenation, through variations in Mn oxide burial, occurring on 10^4-year timescales. The preservation of Mn oxides into sediments can only occur when bottom waters and porewaters are highly oxygen-depleted, due to the reductive dissolution of Mn oxides[34,35] in both the water column and during early burial. Thus, sub-10^6-year shifts in seawater ε^{205}Tl are an indication of changes in the proportion of the ocean bottom water that are oxygen-depleted. Although there is no specific or universal oxygen level below which Mn oxides cease to be preserved in sediments, field data[34,35] suggest that it is likely to be around the hypoxic threshold of ~60 µmol/kg (2 mg/kg), below which O_2 levels are detrimental to most aerobic organisms, with major impacts on the functioning of marine ecosystems[36,37]. Importantly, Sampaio et al.[37] suggest that the ecological impacts of future hypoxic events may be greater than those driven by ocean warming and acidification. During intervals of increased bottom water oxygenation and Mn oxide preservation, ε^{205}Tl will be more negative. Currently, around 5% of the global ocean is hypoxic[38–40] and the ε^{205}Tl of seawater is −6.0[24] due to the expansive, global burial of isotopically positive ε^{205}Tl Mn oxides. Under increasingly hypoxic and anoxic conditions, sequestration of Mn oxide into sediments will decrease and ε^{205}Tl will become less negative, shifting toward the global seawater source value of around −2[25].

Results and discussion

Late Jurassic Palaeoenvironment

The late Jurassic (161–145 Ma) has been thought to be a period of relative climate stability but when atmospheric pCO_2 concentrations were approximately four times the current value[41], resulting in hot and humid 'greenhouse' climate conditions. Sea surface temperatures of ~25–30 °C have been suggested to occur as far south as 60°S[42,43]. In NW Europe, the Upper Jurassic Kimmeridge Clay Formation (KCF) contains a detailed record of sedimentary and oceanographic conditions at this time, specifically for the epicontinental Laurasian Seaway that connected the Arctic and Tethys Oceans[44–47]. Climate reconstructions suggest that the UK sector of the Boreal Sea was a wet and humid, tropical environment, with the Intertropical Convergence Zone (ITCZ) at a latitude of around 35°N[48]. Importantly—and in contrast, for example, to the early Jurassic Toarcian Oceanic Anoxic Event[e.g.49–53]—there is neither carbon isotopic evidence for a notable alteration of the global carbon cycle[54–56], nor evidence for faunal shifts in those marine ecosystems that can be recorded through palaeontological studies[16].

Here, we have analysed sediments deposited between 150 and 149 Ma, from the upper *Pectinatus wheatleyensis* to the lower *Pectinatus pectinatus* ammonite biozones, which are amongst the most organic-rich shales within the KCF in the region, with organic carbon contents averaging 7 wt% (range from 1 to 25 wt%). These samples, from northern England, are stratigraphically correlated to southern England and northern France[44,48,57–59]. The generally high and often exceptionally high abundances of preserved organic matter, along with other geochemical proxies, have been previously used to suggest generally reduced oxygen contents in regional bottom waters, but with fluctuations, from oxic to euxinic, on a range of timescales, including orbitally-paced[45,57,60–65]. However, although there is well-documented evidence for periodic deoxygenation of bottom waters at these sites of major accumulations of sedimentary organic matter[60], the global oxygenation levels of the oceans are unknown on timescales of 10^4–10^6 years, as are any relationships between global and local oxygenation.

Forty samples were taken from the Ebberston (EB) 87 core (Fig. 1) curated by IFP Energies Nouvelles, Chartres, France. The core was drilled in the Cleveland Basin (Yorkshire, UK), one of many small, extensional basins in the epicontinental Laurasian Seaway, which was fully connected to the open ocean at this time[60,66]. With a sampling resolution of around 25,000

years (approximately 1 sample per metre), similar to the modern marine residence time of Tl, this represents one of the highest temporal resolution studies of the global ocean's deoxygenation and reoxygenation, over a period of 1 million years. In addition, more commonly used geochemical proxies allow us to examine the local oxygenation status and to investigate what, if any, constraints can be drawn on global oxygenation from studies at single locations.

Local ocean oxygenation

Most of the study section is described in detail in refs. 60,67, comprises relatively homogenous, bioturbated mudstones that are predominantly composed of detrital quartz, clay minerals and organic matter that, based on its petrographic characteristics and carbon isotopic composition (Fig. 2), has a mainly terrigenous origin. Most trace metal/Al ratios are similar to average shale, as is Fe_T/Al[60] (Fig. 2). However, Mn/Al ratios are much lower than those of average shale and U/Al ratios are slightly elevated[68] (Fig. 2); these ratios suggest that both pore waters and overlying bottom waters were hypoxic. Iron speciation data are also consistent with hypoxia (Fig. 2): Fe_T/Al ratios are close to those of average shale; Fe_{HR}/Fe_T ratios are commonly around 0.4, which is just above the threshold for anoxic bottom waters[21]; Fe_{Py}/Fe_{HR} ratios range from 0.2 to 0.8, which suggests that sediment pore waters were sulphidic but lack strong evidence for euxinia[21].

There are three sedimentologically and geochemically more variable intervals that are highlighted in grey on Fig. 2. These intervals partly comprise similar sediments to those in the main sections but are dominated by two facies that indicate distinctly different local ocean conditions. One is a coccolith-dominated, medium-grained mudstone that includes coccolith-rich faecal pellets, clay minerals, detrital quartz and marine organic matter. The second is an exceptionally organic matter and calcareous pellet-rich, laminated mudstone. Thin section analysis[60,67] shows that, despite exceptionally high concentrations of marine organic matter and strong evidence for high levels of primary productivity (Fig. 2), both sediment types were periodically reworked by—presumably oxygenated—bottom currents. Many of the most organic-rich sediments are highly enriched in iron, with Fe_T/Al ratios above 0.7 and as high as 2.1 (Fig. 2). Values of Fe_T/Al >0.7 indicate an additional, lateral supply of iron to the place of preservation[21]; here, Fe_{HR}/Fe_T ratios >0.5 in the Fe-enriched sediments indicate that much of the additional iron was supplied as oxides, and Fe_{Py}/Fe_{HR} ratios between 0.6 and 0.8 show that much of the reactive iron was converted to, and preserved as, pyrite.

The additional iron was most likely supplied by lateral advection within surface oxygenated waters as a 'particulate shuttle of iron oxide' to locations where conversion to, and preservation as pyrite occurred where pore waters and/or bottom waters were sulphidic[60,69,70]. This is supported by high ratios of Mo/U in the most Fe-enriched sediments (Fig. 2). As redox-sensitive elements, both Mo and U are preferentially preserved in anoxic and sulphidic bottom/pore waters, but Mo is a much more particle-reactive element than U and is, thus, preferentially supplied to areas of deposition sorbed to iron oxides within the shuttle[66,69]. Periodically euxinic local conditions are possible but unproven, although photic zone anoxia has been suggested by the presence of isorenieratene in laterally equivalent sediments from southern England[64].

Global ocean deoxygenation and reoxygenation

ε^{205}Tl values range from −6.6 to −2.9, with most data between −6.6 and −5.3. Fluctuations in ε^{205}Tl occur on different timescales and are not simply related to sedimentology or the redox-sensitive geochemical intervals discussed above (Fig. 2). Broad trends in the data, marked as Sections i to v on Fig. 2, are: (i) an increase in ε^{205}Tl from −6.4 to −3.4 between 72 and 63 m; (ii) the most positive values of −4.2 to −2.9 between 63 and 55.7 m; (iii) a decrease in ε^{205}Tl from −3.1 to −6.0 between 55.7 and 50.0 m; (iv) fluctuations between −6.6 and −4.2 between depths 50.0 and 40.5 m; and (v) an increase in ε^{205}Tl from −6.6 to −4.1 between 41.5 and 31.1 m (Fig. 2). Within these broad trends, one ε-unit differences are common between samples, with a maximum shift of 2.4 ε-units between samples at 55.7 and 54.3 m depth.

The most negative ε^{205}Tl value (−6.6 ± 0.3) is similar to modern-day seawater (−6.0 ± 0.3), suggesting that at certain times (e.g. lower part of Section i and parts of Sections iv and v, Fig. 2), Mn oxide burial rates were similar to those in the modern ocean, and that global seawater redox conditions were predominantly oxic. This assumes that other Tl fluxes, such as the alteration of ocean crust had near-modern values. Whilst the rate of production of ocean crust in the Jurassic was ca. 25% greater than today's value[71], the effect of a 25% increase in the removal rate of Tl into ocean crust is only to shift ε^{205}Tl of seawater by <1 ε-unit[25], so that greater shifts in ε^{205}Tl require a change in the rate of Mn oxide burial. Furthermore, on the 1 Myr time scale of this study, the production rate of ocean crust is effectively constant, so that shifts in ε^{205}Tl in this study relate specifically to changes in the burial rate of Mn oxides. We do, however, note that Mn/Al ratios throughout the section are much lower than average shale[68], suggesting that locally, bottom waters were at least hypoxic, much like oxygen minimum zones on the eastern edges of modern ocean basins; as noted previously, around 5% of the modern ocean is considered hypoxic[38–40].

If ε^{205}Tl values of -6.6 are indicative of ocean bottom waters that are almost entirely oxic and can thus preserve Mn oxides throughout (as interpreted in ref. 25 prior to the Toarcian Oceanic Anoxic Event), deviations in ε^{205}Tl to more positive values can be used to infer increasing deoxygenation of the global ocean. As outlined in the Methods and Supplementary Fig. 1, an oceanic Tl isotopic mass balance model can be used to estimate global changes in the depositional fluxes of Mn oxides and the extent to which the ocean is hypoxic, with the following four assumptions: (a) ε^{205}Tl values of around −2.0 for oceanic Tl inputs; (b) an average isotopic fraction (Δ^{205}Tl) of −1.2 for the altered oceanic crustal sink, (c) an average Δ^{205}Tl of +16 for the fractionation of Tl isotopes between seawater and sorption onto Mn oxides[29], and (d) a linear relationship between the depositional flux of Mn oxides and the proportion of the ocean floor that does not preserve Mn oxides. For the most positive ε^{205}Tl value of −2.9 (59.7 m, Section ii, Fig. 2), this equates to around 70% less Mn oxide burial. Forty percent of the ε^{205}Tl data are more positive than -5.3, a value which suggests up to ~30% less Mn oxide burial compared to both (a) the maximum burial rates during the 1 Myr period studied here and (b) approximately, the modern ocean. In other words, if the amount of Mn oxide burial directly scales with area, for 400,000 of the million years interrogated in this study, > *ca.* 30% of the ocean bottom was hypoxic.

Previous studies have used large-scale Earth System ocean-atmosphere models to suggest that Jurassic and Cretaceous oceans were highly susceptible to deoxygenation. For example, in the Cenomanian and Toarcian[13,14,72], the models suggest that changes in ocean circulation patterns, controlled by a combination of palaeogeography and orbitally induced variations in deep water formation, result in substantial changes in the spatial patterns of oceanic dissolved oxygen; there are also substantial changes in Tl isotopes[25,28]. The thallium isotopic evidence presented here provides direct evidence supporting the modelling results in terms of the general susceptibility of Jurassic-Cretaceous oceans to extensive deoxygenation, in this case between 150 and 149 Ma. These Tl isotope data are some of the first evidence that demonstrates the reality of geologically rapid fluctuations in global bottom water oxygen, at a resolution suggesting that subtle, difficult to observe changes in ocean circulation caused substantial changes in deep water oxygen levels.

Rates of both deoxygenation and reoxygenation of bottom waters vary substantially. For example, between 72 and 66.3 m (Section i, Fig. 2), a period of ca. 130 kyr assuming a constant sedimentation rate of 40 m/Ma, ε^{205}Tl increases from −6.4 to −5.5. This suggests an ocean in which hypoxic bottom waters increase from 5 to 26% of ocean area, assuming that Mn-oxide burial is distributed homogenously throughout an oxic ocean. The average, long-term rate of deoxygenation is then 0.007% per 50 yr, 300 times slower than the current 2% deoxygenation over the last 50 years[1,73].

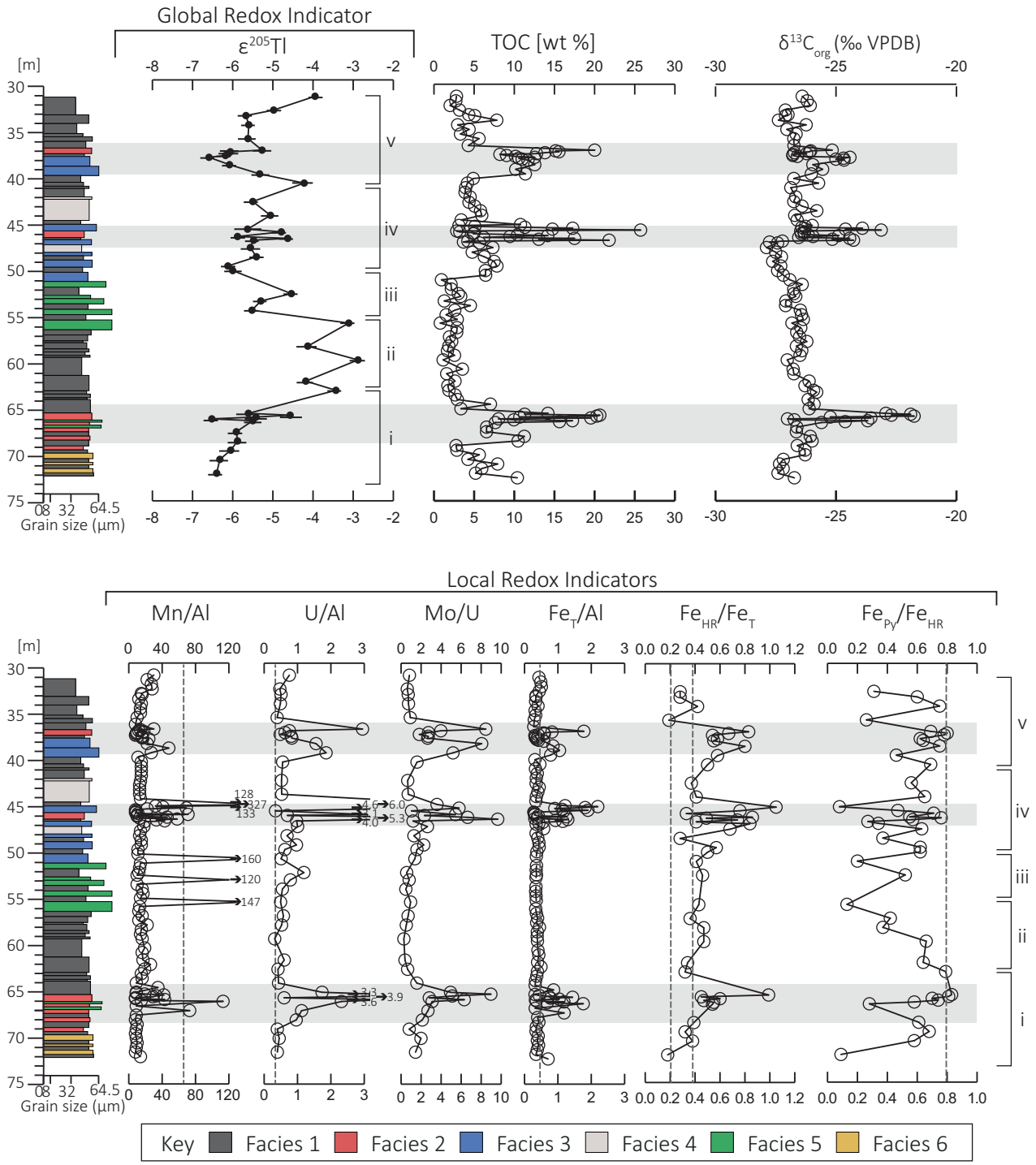

Fig. 2 | Geochemical redox indicators, total organic carbon (TOC), $\delta^{13}C_{org}$, and facies log of the Ebberston-87 core, 150–149 Ma. $\varepsilon^{205}Tl$ data (this study; 2σ analytical errors are shown as horizontal bars) are divided into five sections indicated in the Tl isotope panel as i to v; see text for description and discussion. Note that shifts to less negative $\varepsilon^{205}Tl$ values indicate less preservation of Mn oxides and related deoxygenation of bottom waters (see Methods and Supplementary Fig. 1 for model details). Fe speciation data (this study), and redox sensitive trace elements[60] (Mn/Al, U/Al, and Mo/Al; ppm/wt %). Fe_{HR} highly reactive iron, Fe_T total iron, Fe_{Py} iron bound in pyrite (this study). Dashed vertical lines on Mn/Al, U/Al and Fe_T/Al are values for global average Phanerozoic shale[68]. Dashed vertical lines on Fe_{HR}/Fe_T are values suggested to differentiate oxic (<0.21) environments from **a** possibly anoxic (0.21–0.38) and **b** ferruginous (>0.38)[21]. Dashed vertical line on Fe_{Py}/Fe_{HR} is the value (>0.8) suggested to differentiate euxinic environments from non-euxinic environments[21]. Three periods with much higher TOC contents and isotopically heavier organic matter are indicated with grey shading. They represent times of enhanced preservation of marine organic matter, against a background of isotopically lighter, terrestrial organic matter. Facies 1: Clastic, detritus-rich, medium-grained mudstone; Facies 2: Organic material and calcareous pellet-rich, laminated mudstone; Facies 3: Coccolith-dominated medium mudstone; Facies 4: Agglutinated foraminifera-bearing, medium to coarse, carbonaceous mudstone; Facies 5: Biogenic detritus-dominated, fine to medium mudstone (see ref. 67).

From 37.7 to 31.1 m (Section v, Fig. 2), ε^{205}Tl shifts from −6.1 to −4.0, a change from almost fully oxic bottom waters to 55% hypoxic, at a rate of 0.018% per 50 y, 100 times slower than that in the last 50 years. The most rapid deoxygenation occurs between 66.1 and 65.7 m (Section i, Fig. 2), where ε^{205}Tl shifts from −6.5 to −4.6. Over 10,000 years, the ocean changed from having almost fully oxic bottom waters to 40% hypoxia, at an average rate of 0.2% per 50 yr. Partial reoxygenation occurred immediately afterwards (Section i, 65.7 to 65.5 m), with hypoxic areas decreasing from 40 to 25% over *ca*. 5000 years; a similar oxygenation rate to the prior deoxygenation. These data suggest that hypoxic bottom waters periodically extended into the abyssal plain bottom waters, assuming Mn oxide burial occurs in all depositional environments equally. Whilst in the Jurassic, higher sea levels would mean that the continental shelf was larger than today, only 16% of the modern ocean comprises continental shelf and slope, and 70% of the modern ocean is abyssal plains.

A change over 10,000 years, from an ocean with almost fully oxic bottom waters to one in which 40% of bottom waters were hypoxic, represents a deoxygenation rate that is similar to or even faster than that observed in the period directly leading up to OAE-2[28]. Unlike OAE-2, however, there is no global carbon isotope evidence at 150–149 Ma for a notable change in the global carbon cycle, which might suggest global, anoxia-related preservation of organic matter. Whilst there are major spikes in the isotopic composition of organic carbon seen in Fig. 2, these specifically reflect the enhanced preservation of isotopically distinct marine organic matter against the background of terrestrial organic matter in the rest of the section[60,67], and is, thus, a local record and not indicative of a global increase in organic carbon preservation.

It is important to recognise that deoxygenation rates estimated from ε^{205}Tl in the geological record are strictly changes in the rate of Mn oxide burial, with the assumption of a linear relationship between Mn oxide burial (related to the area of deoxygenated bottom water and sediment) and ocean deoxygenation. In contrast, the calculation of the rate of deoxygenation of the modern ocean is based on volume[1], so that the ancient and modern deoxygenation rates are not strictly comparable. Whilst caution is needed in comparing ancient and modern, the current, 2% deoxygenation rate measured over the last 50 years[1,73] is an order of magnitude faster than the rates estimated in this study of the late Jurassic. We also note that with a longer-term future perspective (10^4–10^5 years), modelling studies[74] suggest that continued global warming will lead to the expansion of oxygen-deficient waters to areas similar to those observed both during OAEs and in this study.

Local vs. global ocean oxygenation

The data plotted in Fig. 2 show no clear relationships between global oxygenation, expressed as variations in ε^{205}Tl, and the sedimentology, organic carbon (OC) content or redox-related geochemistry of the sediments[60] (see full dataset in Supplementary Data, and in Supplementary Tables 1 and 2). ε^{205}Tl values in the homogeneous sections with lower organic matter contents (broadly, TOC < 5%; $\delta^{13}C_{org}$ < 26 ‰), range from −6.0 to −2.9, indicating that these sediments were deposited in a global ocean that had bottom waters that ranged from being almost fully oxic to ones that were ~70% hypoxic (Fig. 2). Locally, these sections are characterised by (i) hypoxic redox conditions based on the local redox indicators (Fig. 2), (ii) OC contents of 1–3% dominated by terrestrial Type III organic material, (iii) an absence of blooms in primary productivity, and (iv) relatively low depositional energy[60,67].The ε^{205}Tl data show that these conditions occurred at times when the global ocean was both well oxygenated and poorly oxygenated; in turn, this means that local geochemical and sedimentological observations are not clear indicators of the oxygenation state of the global ocean.

The danger of extrapolating local indicators of oxygenation to the global ocean has previously been inferred from studies of the Toarcian OAE[53,72,75]. Despite being suggested as an OAE based on carbon isotope shifts, there is in fact limited evidence for the development of global ocean anoxia at that time[75]. Although organic carbon burial rates in anoxic/euxinic basins in Europe increased by a factor of five, sites elsewhere likely remained oxic and show limited changes in organic matter enrichment[53]. Nevertheless, a key difference between our study and the Toarcian OAE, is that during the period of our study (150–149 Ma), there is no evidence for a change in the global carbon cycle of sufficient magnitude to be detected through perturbations in carbon isotope records.

The three intervals that include sediments with the highest OC contents (36.9–39.5 m; 45–46.7 m; 65.5–68.5 m) are typically associated with ε^{205}Tl values from −6.6 to −4.6, and thus a more oxygenated global ocean than the lower OC intervals. During these three periods, in which the preservation of marine organic matter is greatly enhanced, ε^{205}Tl values fluctuate rapidly, with shifts of 1 ε-unit over *ca*. 10,000 years, corresponding to a 20 % change in global, bottom water hypoxia (Fig. 2). There is no relationship between ε^{205}Tl and the local OC contents and redox proxies of the sediments, so the link between local and global oxygenation is highly ambiguous. A generally more oxygenated water column during these periods is consistent with a more vigorous ocean circulation that is recorded in these sediments by erosive events and by sediment deposition from bottom water currents[60]. Oscillations between the higher/lower variable mudstone intervals on the shallow, epicontinental Laurasian seaway have previously been attributed to orbitally modulated shifts in the position of the ITCZ[48]. As a result of movements in the ITCZ, it is possible that cyclone frequency in this region was higher during the higher variability periods than during the periods over which the majority of the sediments were deposited[76], explaining the common observations of sediment transport and erosion during these intervals. A more vigorous circulation is also consistent with enhanced upwelling and nutrient supply to the epicontinental shelf, enhancing primary productivity and resulting in both the coccolith-rich and OC-rich sediments—and in some cases, locally, to euxinic bottom waters.

Conclusions

In a period of hot and humid climate between 150 and 149 Ma, geologically rapid fluctuations in ocean Tl isotope records indicate several episodes when there appears to have been reductions of up to 70% in the global burial of Mn oxides, suggesting major expansions of hypoxic bottom waters. While these fluctuations in Mn oxide burial and deoxygenation occurred on timescales of 10^4–10^5 years, the rates of deoxygenation are still an order of magnitude lower than those occurring in the modern ocean.

At the same time, there are no dramatic changes in the global carbon cycle to sufficiently perturb carbon isotope signatures recorded in organic or inorganic carbon records. This suggests that the ocean can have lower Mn-oxide burial and thus likely lower marine oxygen conditions, that may not lead to substantially increased global burial of OC and a subsequent shift in the isotopic composition of atmospheric and marine carbon. Furthermore, those periods between 150 and 149 Ma during which the global ocean was more hypoxic do not coincide with times of maximum enrichment of sedimentary organic matter in NW Europe. This emphasises the importance of local oceanographic conditions on the production and preservation of organic matter and warns against giving local to regional studies a global significance without more context.

Overall, the combination of carbon and thallium isotope data suggests that marine (de)oxygenation might be more dynamic throughout the Phanerozoic than previously thought, indicating the need to understand how 'normal' or 'baseline' oxygenation conditions may have fluctuated throughout the geologic record, and not only during widely documented OAEs. Equally, the expansion of hypoxic waters, as revealed here by Tl isotopes, may have profound consequences for the biology and biogeochemistry of the oceans, both in the geological past[77]— and into a warmer future.

Methods

This study builds on the geochemical and petrographic studies reported in refs. 60,67, which can be referred to for further detail. Additional data presented in this paper are the analysis of 49 samples for Fe speciation and

42 samples for Tl isotope composition; assuming a constant sedimentation rate, the sampling frequency is approximately 25 kyr.

Sequential iron extraction

Sequential iron extraction was conducted upon 100–200 mg of sample following the methods in ref. 20, operationally defining 'highly reactive' iron (Fe_{HR}) and pyrite Fe (Fe_{Py}). In summary, the first step used a sodium acetate solution, buffered to pH 4.5 with acetic acid, to extract the carbonate phases of the sample (e.g. $FeCO_3$ and $Ca(Fe, Mg, Mn,(CO_3)_2)$). Sodium dithionite, buffered to pH 4.8 with 0.35 M acetic acid and 0.2 M sodium citrate, was then used to extract the Fe associated with crystalline oxides (e.g. FeOOH and Fe_2O_3). Then, Fe in the magnetite (Fe_3O_4) was extracted from the sample using 0.2 M ammonium oxalate, 0.17 M oxalic acid buffered to pH 3.2 to ammonium hydroxide. The supernatant was collected after each extraction and diluted appropriately prior to analysis. Fe concentrations were determined using an Agilent 7500cs inductively coupled plasma spectrometer. Chromium reducible sulphide extraction was carried out following the methods outlined in ref. 79. Pyritic sulphur was extracted by heating 500 mg of sample with a chromium chloride and hydrochloric acid solution for two hours. The evolved hydrogen sulphide gas was passed through a sodium citrate trap and precipitated as silver sulphide (ZnS), which was filtered, dried, and weighed and used to calculate wt% pyrite sulphur stoichiometrically.

Thallium isotopes

Forty two samples were analysed for Tl isotopes following the analytical procedure in ref. 24. Fifty milligrams of sample was treated with 2 M HNO_3 at 130 °C for 12 h to remove the authigenic component of Tl. Samples were centrifuged multiple times and the supernatant (i.e. authigenic component) was collected and treated with HNO_3 and HCl to remove organic material. Anion exchange chromatography was conducted to purify the Tl and quantitatively remove Pb using a single micro-column method and AG1X8 anion exchange resin from Biorad. Tl isotope compositions were measured using a Thermo Scientific Neptune multi-collector inductively coupled plasma mass-spectrometer. Thallium isotopic compositions are compared to the NIST 997 thallium metal standard and reported as:

$$\varepsilon^{205}\mathrm{Tl} = ({}^{205}\mathrm{Tl}/{}^{203}\mathrm{Tl}_{\mathrm{sample}} - {}^{205}\mathrm{Tl}/{}^{203}\mathrm{Tl}_{\mathrm{NIST997}})/({}^{205}\mathrm{Tl}/{}^{203}\mathrm{Tl}_{\mathrm{NIST997}}) \times 10,000$$

with an analytical error for the SCo-1 geostandard of ±0.3 ε units, the long-term laboratory analytical uncertainty. All analyses were conducted in the National High Magnetic Field Laboratory at Florida State University.

Ocean Tl isotope mass balance and estimation of Mn oxide burial in sediments

We use an isotope mass-balance model[27] to estimate changes in the burial of Mn oxides inferred from observed shifts in the Tl composition of seawater:

$$\varepsilon_{SW} = \varepsilon_{IN} - \Delta_{MnOx} + (\Delta_{MnOx} - \Delta_{AOC})((F_{MnOx}/F_{AOC}) + 1) \quad (1)$$

where ε_{SW} and ε_{IN} are the Tl isotope compositions of seawater and total inputs respectively; Δ_{MnOx} and Δ_{AOC} are the isotopic differences between seawater and Mn oxides, and seawater and altered oceanic crust (AOC), respectively; F_{MnOx} and F_{AOC} are the relative fluxes of seawater Tl removal via Mn oxides and altered oceanic crust, respectively. The Tl isotope composition of marine inputs is effectively constant, as are the Tl isotope fractionation factors associated with sorption of Tl by Mn oxides, and the alteration of ocean crust[27]. Because the Tl isotopic composition of marine inputs is constant, it is the relative removal rate of Tl from seawater by Mn oxides and AOC, and how this changes, that governs the Tl isotope composition of seawater. The production rate of ocean crust in the Jurassic was around 25% higher than it is today, so that F_{AOC} may have been similarly enhanced. However, a 25% increase in the flux of Tl into altered ocean crust would only change ε_{sw} by less than one ε-unit (see ref. 27). Furthermore, F_{AOC} depends directly on the long-term (multi-million year) average ocean crust production rate, which can be assumed to be effectively constant over time scales shorter than one million years, as for this study. Here, therefore, changes in the Tl isotope composition of seawater depends almost exclusively on the rate of Tl burial associated with Mn oxides.

Assuming Tl isotopic fractionation values of (a) −1.2 ε-units for the alteration of ocean crust and (b) + 16 ε-units for sorption by Mn oxides and their preservation in marine sediments[24,27,29], Eq. 1 can be used to show how ε_{sw} changes as a result of changes in the flux (preservation rate) of Mn oxides, assuming that F_{AOC} is constant. This is shown in Supplementary Fig. 1.

Reporting summary

Further information on research design is available in the Nature Portfolio Reporting Summary linked to this article.

Data availability

The geochemical dataset generated for and analysed within this study is available in the Figshare repository at https://doi.org/10.6084/m9.figshare.32144395. More geochemical data related to these samples are available in the PANGAEA data repository at https://doi.org/10.1594/PANGAEA.903744.

Received: 27 March 2024; Accepted: 8 May 2026;
Published online: 27 May 2026

References

1. Schmidtko, S., Stramma, L. & Visbeck, M. Decline in global oceanic oxygen content during the past five decades. *Nature* **542**, 335–339 (2017).
2. Keeling, R. F., Körtzinger, A. & Gruber, N. Ocean deoxygenation in a warming world. *Annu. Rev. Mar. Sci.* **2**, 199–229 (2010).
3. Long, M. C., Deutsch, C. & Ito, T. Finding forced trends in oceanic oxygen. *Glob. Biogeochem. Cycles* **30**, 381–397 (2016).
4. Oschlies, A., Brandt, P., Stramma, L. & Schmidtko, S. Drivers and mechanisms of ocean deoxygenation. *Nat. Geosci.* **11**, 467–473 (2018).
5. Laffoley, D. & Baxter, J. (eds.) Ocean deoxygenation: everyone's problem - causes, impacts, consequences and solutions https://doi.org/10.2305/IUCN.CH.2019.13.en (IUCN, Gland, Switzerland, 2019).
6. Deutsch, C., Ferrel, A., Seibel, B., Pörtner, H.-O. & Huey, R. B. Climate change tightens a metabolic constraint on marine habitats. *Science* **348**, 1132–1135 (2015).
7. Wishner, K. F. et al. Ocean deoxygenation and zooplankton: very small oxygen differences matter. *Sci. Adv.* **4**, eaau5180 (2018).
8. Jaccard, S. L. & Galbraith, E. D. Large climate-driven changes of oceanic oxygen concentrations during the last deglaciation. *Nat. Geosci.* **5**, 151–156 (2012).
9. Schlanger, S. & Jenkyns, H. Cretaceous oceanic anoxic events: causes and consequences. *Geol. Mijnbouw* **55**, 179–184 (1976).
10. Auderset, A. et al. Enhanced ocean oxygenation during Cenozoic warm periods. *Nature* **609**, 77–82 (2022).
11. Zhou, X. et al. Upper ocean oxygenation dynamics from I/Ca ratios during the Cenomanian-Turonian OAE 2. *Paleoceanography* **30**, 510–526 (2015).
12. Donnadieu, Y., Pucéat, E., Moiroud, M., Guillocheau, F. & Deconinck, J. F. A better-ventilated ocean triggered by Late Cretaceous changes in continental configuration. *Nat. Commun.* **7**, 10316 (2016).
13. Laugié, M. et al. Exploring the impact of Cenomanian paleogeography and marine gateways on oceanic oxygen. *Paleoceanog. Paleoclimatol.* **36**, e2020PA004202 (2021).
14. Sarr, A. C. et al. Ventilation Changes Drive Orbital-Scale Deoxygenation Trends in the Late Cretaceous Ocean. *Geophys. Res. Lett.* **49**, e2022GL099830 (2022).

15. Savrda, C. E., Bottjer, D. J. & Gorsline, D. S. Development of a comprehensive oxygen-deficient marine biofacies model: Evidence from Santa Monica, San Pedro, and Santa Barbara Basins, California Continental Borderland. *AAPG Bull* **68**, 1179–1192 (1984).
16. Oschmann, W. Kimmeridge Clay sedimentation—a new cyclic model. *Palaeogeogr. Palaeoclimatol. Palaeoecol.* **65**, 217–251 (1988).
17. Algeo, T. J. & Liu, J. A re-assessment of elemental proxies for paleoredox analysis. *Chem. Geol.* **540**, 119549 (2020).
18. Brumsack, H.-J. The trace metal content of recent organic carbon-rich sediments: implications for Cretaceous black shale formation. *Palaeogeogr. Palaeoclimatol. Palaeoecol.* **232**, 344–361 (2006).
19. Tribovillard, N., Algeo, T. J., Lyons, T. & Riboulleau, A. Trace metals as paleoredox and paleoproductivity proxies: an update. *Chem. Geol.* **232**, 12–32 (2006).
20. Poulton, S. W. & Canfield, D. E. Development of a sequential extraction procedure for iron: implications for iron partitioning in continentally derived particulates. *Chem. Geol.* **214**, 209–221 (2005).
21. Raiswell, R. et al. The iron paleoredox proxies: A guide to the pitfalls, problems and proper practice. *Am. J. Sci.* **318**, 491–526 (2018).
22. Dickson, A. J. A molybdenum-isotope perspective on Phanerozoic deoxygenation events. *Nat. Geosci.* **10**, 721–726 (2017).
23. Dickson, A. J. et al. Molybdenum-isotope chemostratigraphy and paleoceanography of the Toarcian Oceanic Anoxic Event (Early Jurassic). *Paleoceanography* **32**, 813–829 (2017).
24. Owens, J. D., Nielsen, S. G., Horner, T. J., Ostrander, C. M. & Peterson, L. C. Thallium-isotopic compositions of euxinic sediments as a proxy for global manganese-oxide burial. *Geochim. Cosmochim. Acta* **213**, 291–307 (2017).
25. Them, T. R. et al. Thallium isotopes reveal protracted anoxia during the Toarcian (Early Jurassic) associated with volcanism, carbon burial, and mass extinction. *Proc. Natl. Acad. Sci. USA* **115**, 6596–6601 (2018).
26. Sweere, T. C. et al. Zinc- and cadmium-isotope evidence for redox-driven perturbations to global micronutrient cycles during Oceanic Anoxic Event 2 (Late Cretaceous). *Earth Planet. Sci. Lett.* **546**, 116427 (2020).
27. Nielsen, S. G. et al. Thallium isotope evidence for a permanent increase in marine organic carbon export in the early Eocene. *Earth Planet. Sci. Lett.* **278**, 297–307 (2009).
28. Ostrander, C. M., Owens, J. D. & Nielsen, S. G. Constraining the rate of oceanic deoxygenation leading up to a Cretaceous Oceanic Anoxic Event (OAE-2: ~ 94 Ma). *Sci. Adv.* **3**, e1701020 (2017).
29. Owens, J. D. Application of thallium isotopes: tracking marine oxygenation through manganese oxide burial. *In Elements in Geochemical Tracers in Earth System Science* https://doi.org/10.1017/9781108688697 (Cambridge University Press, 2019).
30. Nielsen, S. G., Rehkämper, M. & Prytulak, J. 2017. Investigation and application of thallium isotope fractionation. *Rev. Mineral. Geochem.* **82**, 759–798 (2017).
31. Nielsen, S. G. et al. Towards an understanding of thallium isotope fractionation during adsorption to manganese oxides. *Geochim. Cosmochim. Acta* **117**, 252–265 (2013).
32. Peacock, C. L. & Moon, E. M. 2012. Oxidative scavenging of thallium by birnessite: explanation for thallium enrichment and stable isotope fractionation in marine ferromanganese precipitates. *Geochim. Cosmochim. Acta* **84**, 297–313 (2012).
33. Rehkämper, M. & Nielsen, S. G. 2004. The mass balance of dissolved thallium in the oceans. *Mar. Chem.* **85**, 125–139 (2004).
34. Klinkhammer, G. P. & Bender, M. L. The distribution of manganese in the Pacific Ocean. *Earth Planet. Sci. Lett.* **46**, 361–384 (1980).
35. Clement, B. G., Luther, G. W. III & Tebo, B. M. Rapid, oxygen-dependent microbial Mn(II) oxidation kinetics at sub-micromolar oxygen concentrations in the Black Sea suboxic zone. *Geochim. Cosmochim. Acta* **73**, 1878–1889 (2009).
36. Ekau, W., Auel, H., Pörtner, H. O. & Gilbert, D. Impacts of hypoxia on the structure and processes in pelagic communities (zooplankton, macro-invertebrates and fish). *Biogeosciences* **7**, 1669–1699 (2010).
37. Sampaio, E. et al. Impacts of hypoxic events surpass those of future ocean warming and acidification. *Nat. Ecol. Evol.* **5**, 311–321 (2021).
38. Helly, J. J. & Levin, L. A. Global distribution of naturally occurring marine hypoxia on continental margins. *Deep Sea Res.* **51**, 1159–1168 (2004).
39. Karstensen, J., Stramma, L. & Visbeck, M. Oxygen minimum zones in the eastern tropical Atlantic and Pacific Oceans. *Prog. Oceanogr.* **77**, 331–350 (2008).
40. Paulmier, A. & Ruiz-Pinto, D. Oxygen minimum zones (OMZs) in the modern oceans. *Prog. Oceanogr.* **80**, 113–128 (2009).
41. Sellwood, B. W. & Valdes, P. J. Jurassic climates. *Proc. Geol. Assoc.* **119**, 5–17 (2008).
42. Jenkyns, H., Schouten-Huibers, L., Schouten, S. & Sinninghe Damsté, J. 2012. Warm Middle Jurassic–Early Cretaceous high-latitude sea-surface temperatures from the Southern Ocean. *Clim. Past* **8**, 215–226 (2012).
43. Vickers, M. L., Bajnai, D., Price, G. D., Linckens, J. & Fiebig, J. Southern high-latitude warmth during the Jurassic–Cretaceous: New evidence from clumped isotope thermometry. *Geology* **47**, 724–728 (2019).
44. Atar, E., März, C., Schnetger, B., Wagner, T. & Aplin, A. Local to global controls on the deposition of organic-rich muds across the Late Jurassic Laurasian Seaway. *J. Geol. Soc.* **176**, 1143–1153 (2019).
45. Hesselbo, S. P., Deconinck, J.-F., Huggett, J. M. & Morgans-Bell, H. S. 2009. Late Jurassic palaeoclimatic change from clay mineralogy and gamma-ray spectrometry of the Kimmeridge Clay, Dorset, UK. *J.Geol. Soc.* **166**, 1123–1133 (2009).
46. Macquaker, J. H. S., Keller, M. A. & Davies, S. J. Algal blooms and marine snow: mechanisms that enhance preservation of organic carbon in ancient fine-grained sediments. *J. Sed. Res.* **80**, 934–942 (2010).
47. Morgans-Bell, H. S. et al. Integrated stratigraphy of the Kimmeridge Clay Formation (Upper Jurassic) based on exposures and boreholes in south Dorset, UK. *Geol. Mag.* **138**, 511–539 (2001).
48. Armstrong, H. A. et al. Hadley circulation and precipitation changes controlling black shale deposition in the Late Jurassic Boreal Seaway. *Paleoceanography* **31**, 1041–1053 (2016).
49. Hesselbo, S. P. et al. Massive dissociation of gas hydrate during a Jurassic oceanic anoxic event. *Nature* **406**, 392–395 (2000).
50. Remírez, M. N. & Algeo, T. J. Paleosalinity determination in ancient epicontinental seas: a case study of the T-OAE in the Cleveland Basin (UK). *Earth Sci. Rev.* **201**, 103072 (2020).
51. Röhl, H. J., Schmid-Röhl, A., Oschmann, W., Frimmel, A. & Schwark, L. The Posidonia Shale (Lower Toarcian) of SW-Germany: an oxygen-depleted ecosystem controlled by sea level and palaeoclimate. *Palaeogeogr. Palaeoclimat. Palaeoecol.* **165**, 27–52 (2001).
52. Wignall, P. B., Newton, R. J. & Little, C. T. The timing of paleoenvironmental change and cause-and-effect relationships during the Early Jurassic mass extinction in Europe. *Am. J.Sci.* **305**, 1014–1032 (2005).
53. Kemp, D. B., Suan, G., Fantasia, A., Jin, S. & Chen, W. Global organic carbon burial during the Toarcian oceanic anoxic event: Patterns and controls. *Earth Sci. Rev.* **231**, 104086 (2022).
54. Jelby, M. E. et al. Arctic reappraisal of global carbon-cycle dynamics across the Jurassic–Cretaceous boundary and Valanginian Weissert Event. *Palaeogeogr. Palaeoclimatol. Palaeoecol.* **555**, 109847 (2020).
55. Price, G. D., Főzy, I. & Pálfy, J. 2016. Carbon cycle history through the Jurassic–Cretaceous boundary: A new global $\delta^{13}C$ stack. *Palaeogeogr. Palaeoclimatol. Palaeoecol.* **451**, 46–61 (2016).

56. Weissert, H. & Erba, E. Volcanism, CO_2 and palaeoclimate: a Late Jurassic–Early Cretaceous carbon and oxygen isotope record. *J. Geol. Soc.* **161**, 695–702 (2004).
57. Cox, B. M. & Gallois, R. W. The stratigraphy of the Kimmeridge Clay of the Dorset type area and its correlation with some other Kimmeridgian sequences. *Rep. Instit. Geol. Sci.* **80/4**, 1–44 (1981).
58. Herbin, J., Muller, C., Geyssant, J., Mélières, F. & Penn, I. Hétérogénéité quantitative et qualitative de la matière organique dans les argiles du Kimmeridgien du Val de Pickering (Yorkshire, UK). *Revue de l'Institut Français du Pétrole* **46**, 675–712 (1991).
59. Oschmann, W. Distribution, dynamics and palaeoecology of Kimmeridgian (Upper Jurassic) shelf anoxia in western Europe. *Geol. Soc. London Spec. Publ.* **58**, 381–395 (1991).
60. Atar, E. et al. Dynamic climate-driven controls on the deposition of the Kimmeridge Clay Formation in the Cleveland Basin, Yorkshire, UK. *Clim. Past* **15**, 1581–1601 (2019).
61. Pearce, C. R., Coe, A. L. & Cohen, A. S. Seawater redox variations during the deposition of the Kimmeridge Clay Formation, United Kingdom (Upper Jurassic): evidence from molybdenum isotopes and trace metal ratios. *Paleoceanography* **25**, PA4213 (2010).
62. Sælen, G., Tyson, R. V., Telnæs, N. & Talbot, M. R. Contrasting watermass conditions during deposition of the Whitby Mudstone (Lower Jurassic) and Kimmeridge Clay (Upper Jurassic) formations, UK. *Palaeogeogr. Palaeoclimatol. Palaeoecol.* **163**, 163–196 (2000).
63. Tyson, R., Wilson, R. & Downie, C. A stratified water column environmental model for the type Kimmeridge Clay. *Nature* **277**, 377–380 (1979).
64. Van Kaam-Peters, H. M. E., Schouten, S., Köster, J. & Sinninghe Damstè, J. S. Controls on the molecular and carbon isotopic composition of organic matter deposited in a Kimmeridgian euxinic shelf sea: evidence for preservation of carbohydrates through sulfurisation. *Geochim. Cosmochim. Acta* **62**, 3259–3283 (1988).
65. Wignall, P. B. Sedimentary dynamics of the Kimmeridge Clay: tempests and earthquakes. *J. Geol. Soc.* **146**, 273–284 (1989).
66. Tribovillard, N., Algeo, T. J., Baudin, F. & Riboulleau, A. Analysis of marine environmental conditions based on molybdenum–uranium covariation—Applications to Mesozoic paleoceanography. *Chem. Geol.* **324–325**, 46–58 (2012).
67. Atar, E., Aplin, A. C., Lamoureux-Var, V., März, C. & Wagner, T. Sedimentation of the Kimmeridge Clay Formation in the Cleveland Basin (Yorkshire, UK). *Minerals* **10**, 977 (2020).
68. Ray, E. & Paul, D. Major and trace element characteristics of the average indian post-archean shale: implications for provenance, weathering, and depositional environment. *ACS Earth Space Chem.* **5**, 1114–1129 (2021).
69. Goldberg, E. D. Marine geochemistry 1. Chemical scavengers of the sea. *J. Geol.* **62**, 249–265 (1954).
70. Tribovillard, N. et al. Iron availability as a dominant control on the primary composition and diagenetic overprint of organic-matter-rich rocks. *Chem. Geol.* **401**, 67–82 (2015).
71. Gernon, T. M. et al. Global chemical weathering dominated by continental arcs since the mid-Palaeozoic. *Nat. Geosci.* **14**, 690–696 (2021).
72. Ruvalcaba Baroni, I. et al. Ocean circulation in the Toarcian (Early Jurassic): a key control on deoxygenation and carbon burial on the European shelf. *Paleoceanogr. Paleoclimatol.* **33**, 994–1012 (2018).
73. Stramma, L., Johnson, G. C., Sprintall, J. & Mohrholz, V. Expanding oxygen-minimum zones in the tropical oceans. *Science* **320**, 655–658 (2008).
74. Ruvalcaba Baroni, I., Palastanga, V. & Slomp, C. P. Enhanced organic carbon burial in sediments of oxygen minimum zones upon ocean deoxygenation. *Front. Mar. Sci.* **6**, 839 (2019).
75. Remírez, M. N. & Algeo, T. J. Carbon-cycle changes during the Toarcian (Early Jurassic) and implications for regional versus global drivers of the Toarcian oceanic anoxic event. *Earth-Sci. Rev.* **209**, 103283 (2020).
76. Colombié, C., Carcel, D., Lécuyer, C., Ruffel, A. & Schnyder, J. Temperature and cyclone frequency in Kimmeridgian Greenhouse period (late Jurassic). *Glob. Planet. Change* **170**, 126–145 (2018).
77. Pohl, A. et al. Continental configuration controls ocean oxygenation during the Phanerozoic. *Nature* **608**, 523–527 (2022).
78. Gröcke, D. R., Price, G. D., Ruffell, A. H., Mutterlose, J. & Baraboshkin, E. Isotopic evidence for Late Jurassic–Early Cretaceous climate change. *Palaeogeogr. Palaeoclimatol. Palaeoecol.* **202**, 97–118 (2003).
79. Canfield, D. E., Raiswell, R., Westrich, J. T., Reaves, C. M. & Berner, R. A. The use of chromium reduction in the analysis of reduced inorganic sulfur in sediments and shales. *Chem. Geol.* **54**, 149–155 (1986).

Acknowledgements

This research was conceived during a PhD funded by Durham University as part of a Natural Environment Research Council Centre for Doctoral Training (grant number NEM00578X/1). We are grateful to IFP Energies Nouvelles, Chartres, France, for permission to obtain samples from the Ebberston (EB) 87 core and thank Chelsea Bowman for assistance in sample processing. We thank Peter Talling for his helpful comments on an early draft of the manuscript, and both the journal reviewers and editors for their substantial efforts to improve the manuscript.

Author contributions

E.A. conceived the study, collected geochemical data and co-wrote the first draft of the manuscript. A.C.A. co-wrote the first draft of the manuscript. S.M.N. provided laboratory supervision and contributed to manuscript review and editing. S.A.Y. provided laboratory supervision and contributed to manuscript review and editing. J.D.O. contributed to manuscript review and editing, and acquired funding. All authors discussed the results and approved the final manuscript.

Funding

This work was funded by grants from the National Science Foundation (EAR-2026926) to JDO, Alfred P. Sloan Foundation FG-2020-13552 (JDO), and the FSU EOAS Winchester Fund for graduate student support (SMN).

Competing interests

The authors declare no competing interests.

Additional information

Supplementary information The online version contains supplementary material available at https://doi.org/10.1038/s43247-026-03640-7.

Correspondence and requests for materials should be addressed to Andrew C. Aplin.

Peer review information *Communications Earth & Environment* thanks the anonymous reviewers for their contribution to the peer review of this work. Primary handling editors: Mojtaba Fakhraee, Alireza Bahadori, and Carolina Ortiz Guerrero. A peer review file is available

Reprints and permissions information is available at http://www.nature.com/reprints

Publisher's note Springer Nature remains neutral with regard to jurisdictional claims in published maps and institutional affiliations.

Open Access This article is licensed under a Creative Commons Attribution 4.0 International License, which permits use, sharing, adaptation, distribution and reproduction in any medium or format, as long as you give appropriate credit to the original author(s) and the source, provide a link to the Creative Commons licence, and indicate if changes were made. The images or other third party material in this article are included in the article's Creative Commons licence, unless indicated otherwise in a credit line to the material. If material is not included in the article's Creative Commons licence and your intended use is not permitted by statutory regulation or exceeds the permitted use, you will need to obtain permission directly from the copyright holder. To view a copy of this licence, visit http://creativecommons.org/licenses/by/4.0/.

© The Author(s) 2026